Atomization and Sprays 20(4), 297–310 (2010)

SPLASHING PHENOMENA DURING LIQUID DROPLET IMPACT

Jie Liu,[1] Henry Vu,[1] Sam S. Yoon,[2,] Richard Jepsen,[3] & Guillermo Aguilar[1,*]*

[1]*Department of Mechanical Engineering, University of California-Riverside, Riverside, California 92521*

[2]*Department of Mechanical Engineering, Korea University, Anamdong, 5-Ga, Sungbukgu, Seoul, 136-713, Korea*

[3]*Sandia National Laboratories, Albuquerque, New Mexico 87185*

[*]Address all correspondence to G. Aguilar and S. S. Yoon E-mail: gaguilar@engr.ucr.edu and skyoon@korea.ac.kr

Original Manuscript Submitted: 16/10/2009; Final Draft Received: 23/2/2010

Splashing is a phenomenon often observed during liquid droplet impact onto a solid surface. The threshold of splashing is known to be related to droplet size, impact velocity, and physical properties of the liquid, but the mechanisms that initiate splashing are not understood completely. In accordance with the Kelvin-Helmholtz (K-H) instability analysis, recent studies have shown that ambient gas density has a significant effect on the threshold and trajectory of splashing. In this study, the effects of droplet velocity, impact angle, and ambient gas pressure (or density) on the threshold of splashing and the motion of the ambient gas surrounding the droplet were examined. Experimental observations of splashing were carried out with a droplet of 1.7 mm in diameter, while varying droplet velocity, impact angle, and ambient pressure. An empirical correlation was derived using our and other published data to determine the threshold of splashing based on the aforementioned parameters. Also, a numerical simulation using the volume of fluid method was carried out to calculate the gas velocities surrounding the droplet during impact. The results of this model gave supportive evidence that K-H instability is a suitable instability theory that helps explain the splash phenomenon with consideration of the gas motion surrounding the droplet.

KEY WORDS: *droplet, impact, splash, instability, splash threshold*

1. INTRODUCTION

The splashing phenomenon that occurs after a liquid droplet impacts onto a solid or liquid surface was first studied by Worthington (1876). Although the physical mechanisms of splashing are still not completely understood, droplet impact against solid and liquid surfaces has been widely used for materials processing, ink printing, spray cooling, and irrigation. Engel (1955) showed that the pressure variation inside the droplet during impact was the key factor that caused splashing. Studies of droplet impacts at velocities over 100 m/s against a rigid surface showed that splashing may be attributed to a pressure-related shockwave, which is initiated due to the compression of the front part of the droplet at the beginning stage of contact against the rigid solid surface (Bowden and Field, 1964; Hobbs and Kezweeny, 1967; Hobbs and Osheroff, 1967; Levin and Hobbs, 1970, 1971; Lesser, 1981; Lesser and Field, 1983; Field et al., 1985). Then, when the momentum of the liquid droplet cannot

1044–5110/10/$35.00

NOMENCLATURE

Ca	capillary number ($V\mu/\sigma$)	t_c	characteristic spreading time, s
C_g	sound speed in ambient gas, m/s	T	temperature, °C
C_l	sound speed in liquid, m/s	$T_{\rm sat}$	saturation temperature of droplet at 1 atm, °C
$\vec{F}$	force, N	V	droplet velocity, m/s
h	thickness of flattened droplet at maximum spread diameter, m	$\vec{V}_n$	impact velocity in normal direction to the impact surface, m/s
k	wave number	$V_{\rm rel}$	relative velocity, m/s
m	mass, kg	V_s	spreading velocity, m/s
M_m	molecular weight of the gas, g/mol	We	Weber number ($D\rho V^2/\sigma$)
n	adiabatic gas constant	**Greek Symbols**	
p	ambient gas pressure, Pa	μ	dynamic viscosity, kg/s m
P_0	atmospheric pressure, 101000 Pa	ν	kinematic viscosity, m^2/s
P	pressure inside droplet, Pa	ω	interface growth rate, m/s^2
r	radius of droplet spread, m	θ	static wetting angle, deg
R_m	maximum spread radius, m	ρ	liquid density, kg/m^3
Re	Reynolds number (ρ/μ)	ρ_g	ambient gas density, kg/m^3
R_u	universal gas constant [8314 N m/kg mol K]	σ	surface tension, N/m
t	time from droplet impact, s	$\tau_{\rm ST}$	shear stress caused by surface tension, N/m^2

convert into the flow momentum along the impact surface during the impact process, splashing occurs at the location where the surface energy is the least (Harlow and Shannon, 1967; Stow and Hadfield, 1981). This assumption has been supported by experimental measurements, which were taken when surface roughness was increased (Range and Feuillebois, 1998a,b; Field, 1999) and when a vertical obstacle was added on the solid surface (Josserand et al., 2005). Both the surface roughness and vertical obstacles reduce the momentum of flow along the impact surface. As a result, the pressure at the front edge of the flow along the impact surface increases to facilitate splashing.

Additionally, Allen (1975, 1988) applied the Rayleigh-Taylor (R-T) instability theory to demonstrate that splashing was one of the products of instability formation. Recent research, however, has shown that Kelvin-Helmholtz (K-H) instability, which is caused by the shear stress between two fluids moving in parallel at a relative velocity, provides a better explanation of splashing than R-T instability theory because it considers the exchange of momentum between the gas underneath and the droplet as the latter is about to impact the solid surface (Kim et al., 2000; Yoon and DesJardin, 2006; Yoon et al., 2007). In this context, Xu (2007) discovered that as the ambient pressure drops to 0.17 atm, splashing could not be observed. A more detailed description of the interaction between a water droplet and ambient gas during impact was presented by Jepsen et al. (2006), who used the Schlieren photography method to observe the gas movement, which varied with the ambient pressure during a water slug impact onto a solid surface. Additionally, Yoon et al. (2009) presented further evidence for K-H instability through imaging of finger formation in droplets impacting into liquid pools where fluid density differences did not exist.

Experimental methods have been applied to find the quantitative threshold of splashing during droplet impact based on the Weber number (We) and the Reynolds number (Re). These studies have related the threshold of splashing to liquid properties, such as the surface tension and viscosity, and also to the impact surface characteristics (Mundo et al., 1995; Rein, 1996; Prunet-Foch et al., 1998; Kang and Lee, 2000; Rioboo et al., 2001, 2003). Kelvin-Helmholtz instability, however, has generally not been considered in splashing threshold correlations, nor has the effect of ambient pressure and impact angle been studied together systematically.

In this study, we observe and record the dynamics of droplets of various fluid properties as they impact against a rigid solid dry surface at different inclination angles,

at pressures ranging from 0.2 to 6 atm. Although they are known to influence impact dynamics, the influence of surface wettability and temperature on splashing threshold was assumed to be small relative to other factors (Li et al., 2009). On the basis of the experimental results, we develop an empirical expression to predict the threshold of splashing that uses the balance between the droplet internal pressure and the droplet surface tension while considering K-H instability and gas pressure. To further validate the applicability of the K-H instability on splashing, a numerical simulation based on a volume of fluid (VOF) algorithm was also performed.

2. METHODS

2.1 Experimental Approach

The liquid used in this study was FC-72 or perfluorohexane (C_6F_{14}), whose properties are shown in Table 1 along with two other commonly used liquids, water and ethanol, for comparison. FC-72 is normally used as an electronic cooling fluid and its selection for the current study provided a wide range of values for We. A diagram of the experimental setup is provided in Fig. 1. A precision microliter valve (Model 740V-SS, EFD Inc., East Providence, Rhode Island) with stainless steel tips of various outer diameters was used to generate droplets of 1.7 mm diameter. The distance from the nozzle tip to the impact surface was varied from 0.06 to 1.32 m to produce impact velocities from 1 to 5 m/s. A smooth Plexiglas surface with less than 0.8 μm in roughness was mounted on a rotary stage (Model B5990TS, Velmex Inc., Bloomfield, New York) at various impact angles ranging from 0 to 45 deg relative to the horizontal plane.

To help quantify the significance of K-H instability, ambient gas pressure was varied from 1 to 6 atm by performing experiments in an aluminum pressure chamber. Dry air was used to vary ambient pressure. All experiments were performed isothermally at 298 K to maintain constant fluid properties and eliminate heat transfer effects. Two clear polycarbonate windows facilitated video imaging of the impact phenomena using a Phantom V7 high-speed video camera (Vision Research, Inc, Wayne, New Jersey) at a rate of 4800–17,021 frames per second. Quantitative results for each condition were determined by averaging four test runs.

2.2 Numerical Simulation

To study how the ambient gas pressure affects splashing during impact, computational fluid dynamics (CFD) software, Fluent 6.3 (Fluent Inc., Lebanon, New Hampshire) was used to simulate the droplet impact, based on an implicit VOF scheme. This scheme simulates multiphase flows by assigning a volume fraction of each phase within each cell. If α_q is the volume fraction of the qth fluid, then values of $\alpha_q = 0$ and $\alpha_q = 1$ represent cells empty and full of the qth fluid, respectively. Values of α_q between 0 and 1 represent interfaces between phases. The interface is tracked using continuity,

$$\frac{\partial \alpha_q}{\partial t} + u_i \frac{\partial \alpha_q}{\partial x_i} = 0$$

The momentum equation is used to solve a single velocity field representing all phases,

$$\frac{\partial}{\partial t}\rho u_j + \frac{\partial}{\partial x_i}\rho u_i u_j = -\frac{\partial P}{\partial x_j} + \frac{\partial}{\partial x_i}\mu\left(\frac{\partial u_i}{\partial x_j} + \frac{\partial u_j}{\partial x_i}\right) + \rho g_j + F_j$$

with fluid properties determined by using volume fraction averages, e.g., for μ,

$$\mu = \sum \alpha_q \mu_q$$

FC-72 droplets of 1.7 mm diameter were generated and allowed to impact at velocities of either 2 or 5 m/s. The droplets impacted onto a horizontal or 45 deg inclined surface at surrounding ambient pressures of 1 or 4 atm. Although the droplet was spherical, a 2D simulation, instead of a full 3D simulation, was performed (Jepsen et al., 2006) to increase the calculation efficiency. It can be reasonably assumed that the impact phenomena are axially symmetric. Therefore, a 2D simulation

TABLE 1: Properties of FC-72 in Comparison to Water and Ethanol

	FC-72	**H_2O**	**CH_3OH**
Density ρ (kg/m^3)	1680	1000	791
Surface tension σ (mN/m)/T	12.0	73	26
Viscosity μ (Pa s)	0.00064	0.000978	0.00058
Boiling point (°C)	56	100	65

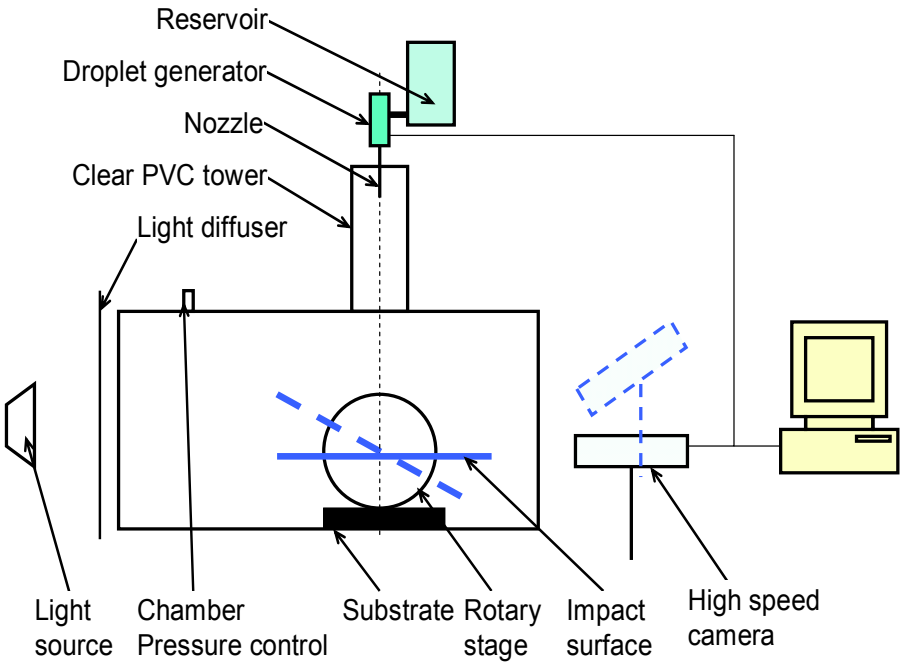

FIG. 1: A schematic diagram of the experimental setup.

through the center of the droplet should adequately resolve the flow phenomena. A rectangular calculation domain of 4 mm in width and 3 mm in height was used, and the initial position of the droplet was set at the center of the calculation domain. Larger domains were tested, but this had no impact on the results during the time period of interest. The boundary condition at the impact surface was a solid wall (Jepsen et al., 2006) and the other three boundary conditions were also set to a solid wall (Fujimoto et al., 2007). For all simulations, the initial velocity of the air was set to 0.

A dynamic mesh was used, with finer element spacing near the impact surface. The governing equations were solved using a fully implicit scheme with a strict convergence criterion, $\varepsilon_n^{l,m} = (U_n^{l,m+1} - U_n^{l,m})/U_n^{l,m} < 10^{-6}$, where n is the element, l is the time step, and m is iteration. The simulation showed good convergence with an error decreasing to 10^{-9} as l increased for each element. A time step of $< 10^{-5}$ s was used in the final simulation.

3. EXPERIMENTAL RESULTS

3.1 Effect of the Weber Number

Figure 2 shows the effect of We on the impact dynamics. For We = 695 (left side), it is observed that the water sheet spreads along the flat surface with no splash. For We = 1870 (right side), however, the edge of the liquid is ejected at a certain angle from the horizontal plane at t = 0.11 ms. At t = 0.32 ms, a crown-shaped splash is clearly observed. At t = 0.85 ms, tiny water droplets are separated from the main crown structure of the liquid.

3.2 Effect of Ambient Pressure

Figure 3 shows a sequence of an FC-72 droplet impact against a flat surface for We = 970 at different values of ambient pressure ranging from 1 to 6 atm. At 1 atm, the FC-72 liquid spreads along the flat surface and no splashing occurs. As the pressure increases to 2 atm, mild splashing is observed at the advancing edge of the spread. The splash droplets also travel a longer distance than the leading edge of the spread on the flat surface. By further increasing the pressure to 4 atm, splashing is observed earlier than that at 2 atm. Splashing is also stronger, and the height of the splashed droplets is larger, but spreading still occurs along the impact surface. At 6 atm, splashing is again more pronounced and develops into a crown shape, which is different from the shape of the splashing at 2 and 4 atm. The bottom of the splash is detached from the flat surface at a large angle. The height of the splashed droplets at 6 atm is also higher than that at 4 atm.

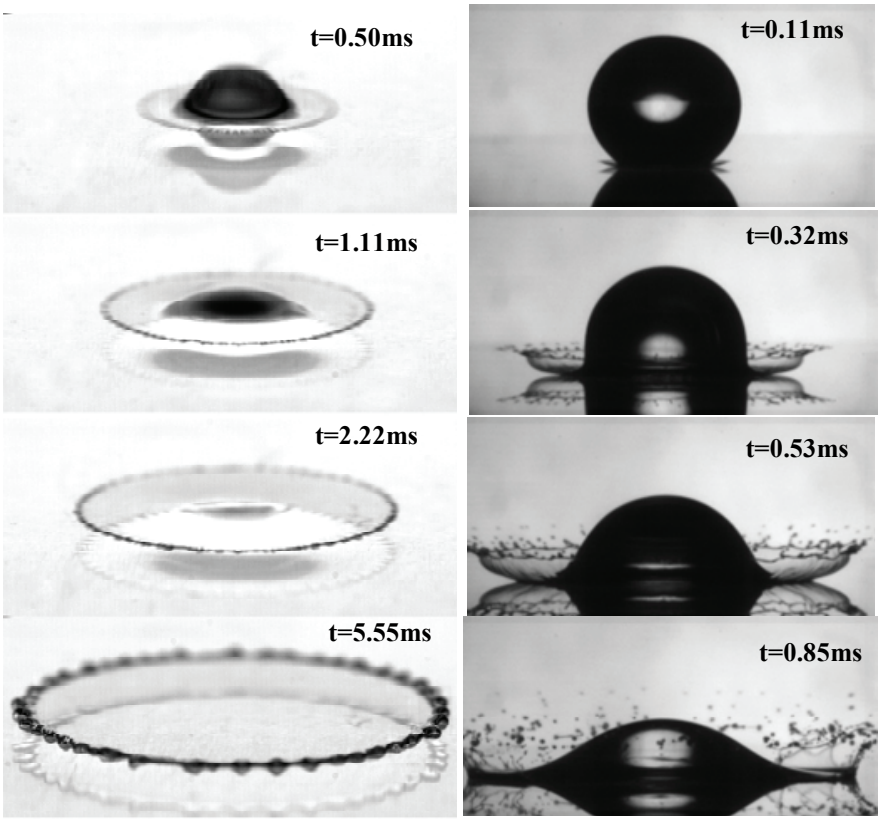

FIG. 2: Effect of We on splashing. Left column, water droplet with We = 695; and right column, ethanol droplet with We = 1870 (Yoon and DesJardin, 2006).

To provide some quantitative description of the splashing phenomenon, the angle between the splashing projectile and the horizontal level was obtained, as shown in Fig. 4a, from a series of high-speed images. Figure 4b shows how the splashing angle increases with increasing ambient pressure for an FC-72 droplet. Splashing angles of 10, 30, 45, and 60 deg correspond to ambient pressures of 1, 2, 4, and 6 atm, respectively. From the weak splashing at 2 atm to the strong crown splashing at 6 atm, it is clear that the ambient pressure has a significant effect on the splashing behavior.

3.3 Effect of Impact Angle

In addition to the ambient pressure, the impact angle is another important parameter affecting the splashing. Figure 5 shows the impact of an FC-72 droplet onto an inclined Plexiglas surface at angles of 15, 30, and 45 deg for We = 970 and air pressure of 3 atm. The arrows show the inclined and normal directions of the impact plate, respectively, and the cross indicates the initial point of contact. At 15 deg, the splash occurs clearly on both sides of the droplet. However, unbalanced splashing is observed with spreading distance, and splash height in the downhill direction is larger than that in the uphill direction. As the inclination angle increases to 30 deg, the magnitude of splashing is much weaker and only occurs in the downhill direction. Again, the displacement of the FC-72 layer is much larger in the downhill direction. At 45 deg, the splashing is nearly eliminated, but with significantly higher overall spreading displacement downhill.

The velocities in the downhill and uphill directions were measured by using image measurement software as shown in Fig. 6. The downhill velocity is larger than the uphill velocity for all the inclined surfaces. At t = 70 μs, the dimensionless velocities (V_s/V, where V_s is the spreading velocity of the liquid sheet and V is the impact velocity) in the downhill and uphill directions are 3.65 and 3.17 for 15 deg, 3.99 and 2.83 for 30 deg, and 4.54 and 2.81 for 45 deg. Thus, the differences of

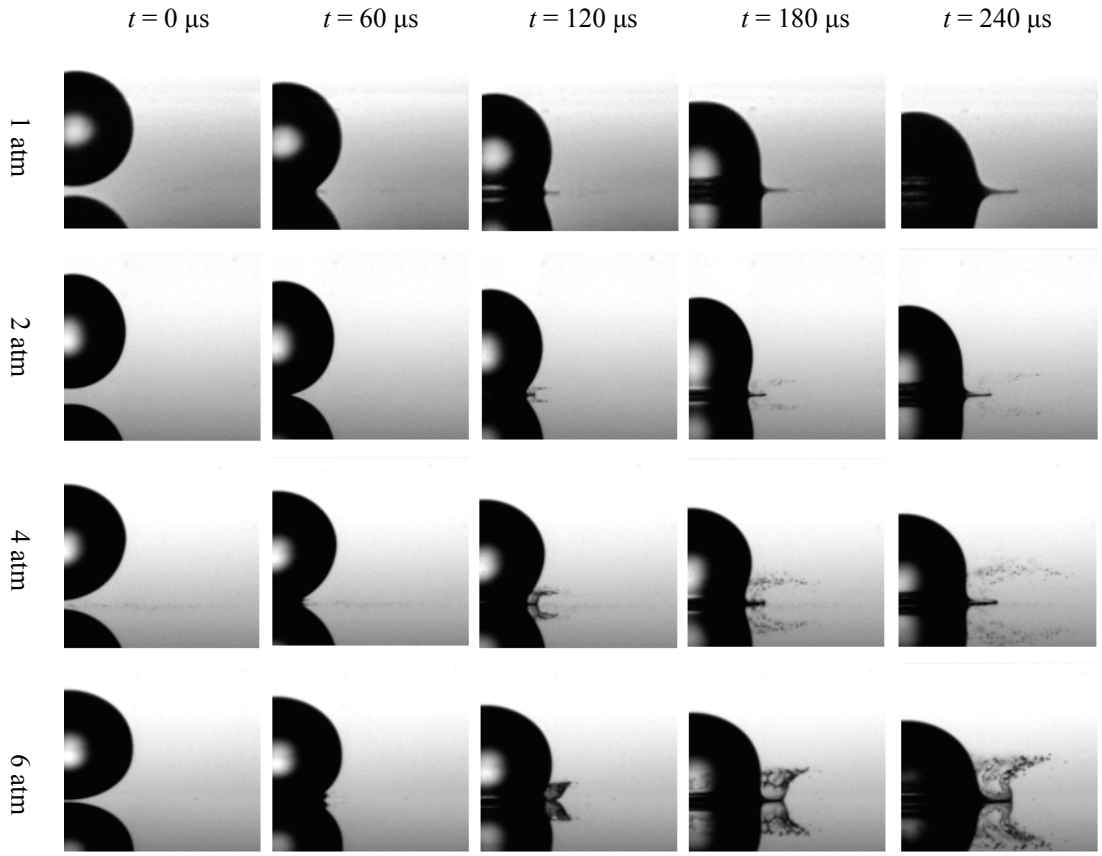

FIG. 3: Effect of ambient air pressure on splashing with FC-72 droplet with We = 970 and Re = 8700 with pressure at 1, 2, 4, and 6 atm for frames at each row.

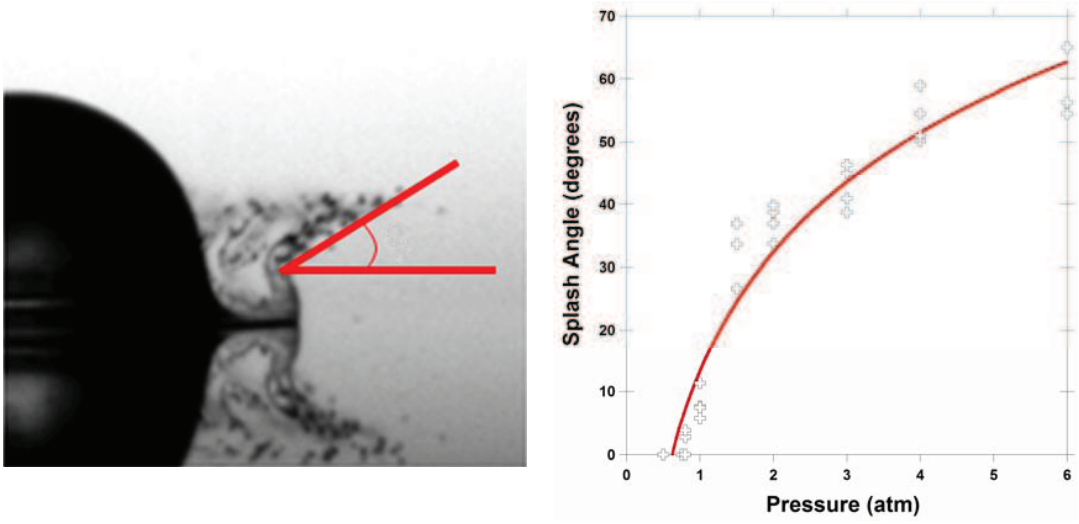

(a) (b)

FIG. 4: (a) A depiction of the method of splash angle measurement. (b) Splash angle increases as the ambient pressure increases with FC-72 droplet with We = 970 and Re = 9620.

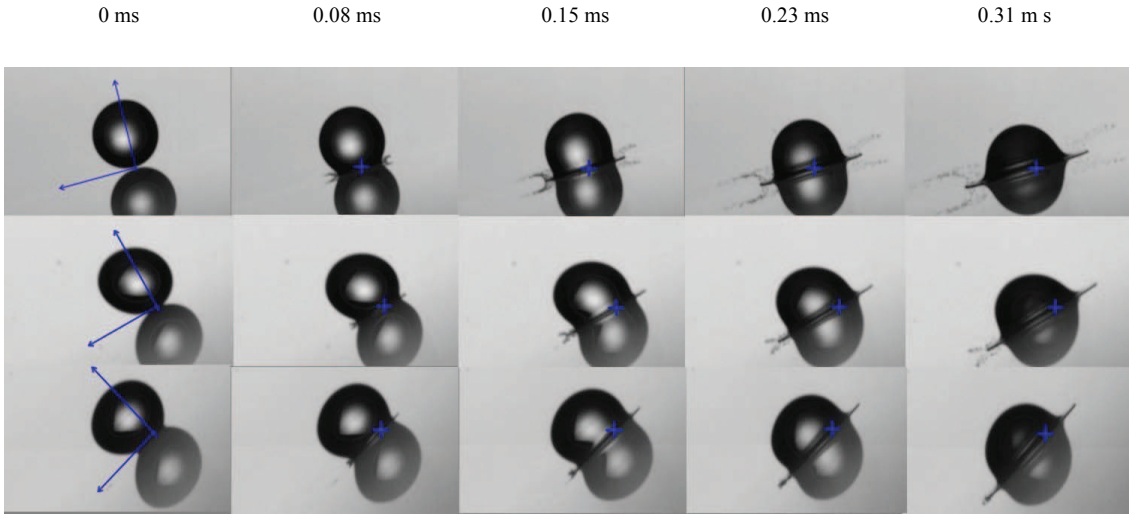

FIG. 5: Effect of angle of impact surface. Top, inclined angle 15 deg; middle, inclined angle 30 deg; and bottom, inclined angle 45 deg with FC-72 droplet with We = 970 and Re = 8700 at 3 atm. The marked cross is an impact point.

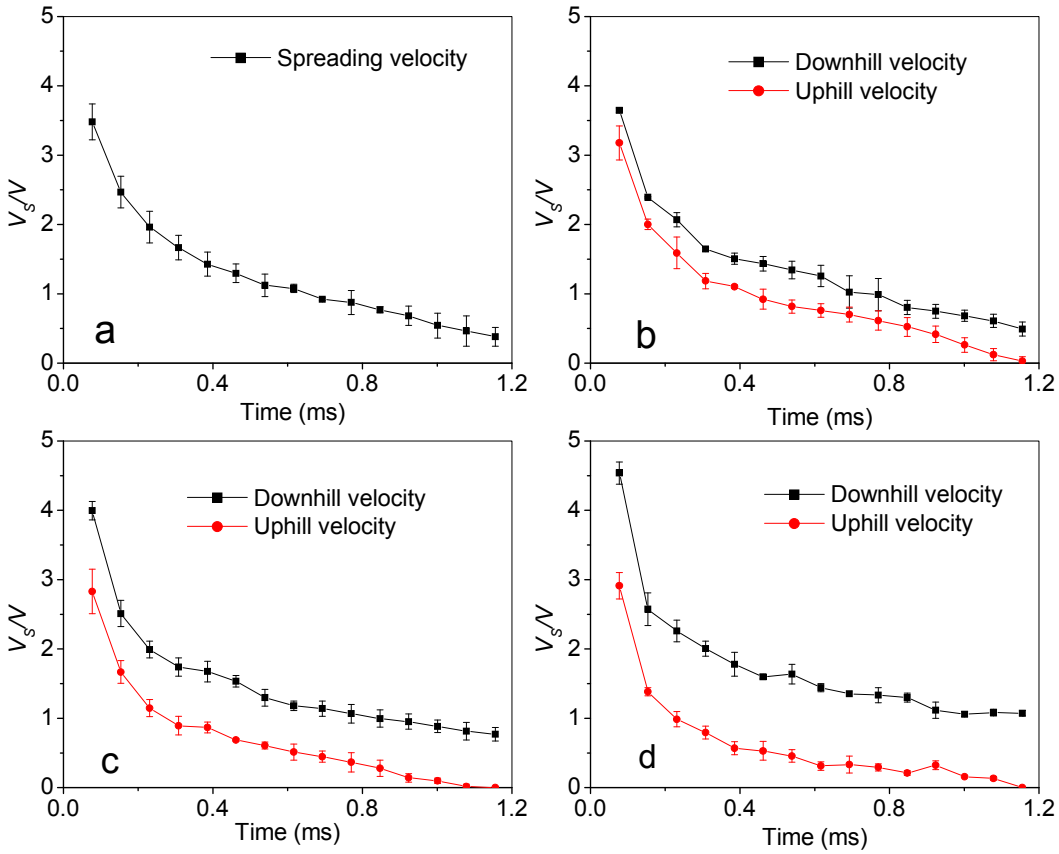

FIG. 6: Spreading velocity of downhill and uphill with FC-72 droplet with We = 970 and Re = 8700 impact onto (a) flat surface, (b) 15 deg, (c) 30 deg, and (d) 45 deg angle Plexiglas.

the dimensionless velocity between the downhill and uphill directions are 0.48, 1.16, and 1.78, respectively. At 1.2 ms after impact, the dimensionless velocities uphill are about 0 for all three cases of inclined surfaces, but the dimensionless downhill velocities are 0.6, 1.1, and 1.4 for inclination angles of 15, 30, and 45 deg, respectively.

4. NUMERICAL RESULTS

Figures 7a and 7b show the simulation of air movement near the droplet of D = 1.7 mm just in contact with the substrate at ambient pressures of 1 and 4 atm, respectively. The impact velocity V is 2 m/s for We = 970 and Re = 8700. The solid curve shows the contour of the droplet as it establishes contact with the surface. At this stage, the spreading or splashing has not yet occurred, and the front edge of the droplet flattens at the contact area. The air between the droplet and the impact surface moves outward quickly near the contact area.

The effect of the ambient pressure on the magnitude and angle of the air velocity vectors is also shown. Increasing the value of the ambient pressure reduces the maximum air velocity from 30.4 m/s at 1 atm to 26.4 m/s at 4 atm, but the air velocity angle increases with pressure. Figure 7c shows that the air velocity near the contact area of the droplet moving at V = 5 m/s and 1 atm is much greater than that of the droplet moving at V = 2 m/s. As V increases from 2 to 5 m/s, the movement of the air near the contact point increases dramatically; the maximum velocity of the air is about 30 m/s for the droplet impacting at V = 2 m/s, and it reaches a value over 80 m/s when the droplet impacts at V = 5 m/s.

Figure 8 shows that at the impact angle of 45 deg for V = 2 m/s, the maximum air velocity in the downhill direction is only 22 m/s, while it is less than 10 m/s in the uphill direction; both being lower than the corresponding air velocity seen for impacts on a horizontal surface (∼30 m/s), as seen in Fig. 7.

Figure 9 shows the simulated pressure profile inside the droplet. Some aberrations in the droplet boundary can be seen, and these occurred due to the change in mesh spacing, but this is far from the area of interest and did not affect the results. Figure 9a shows the case of a droplet

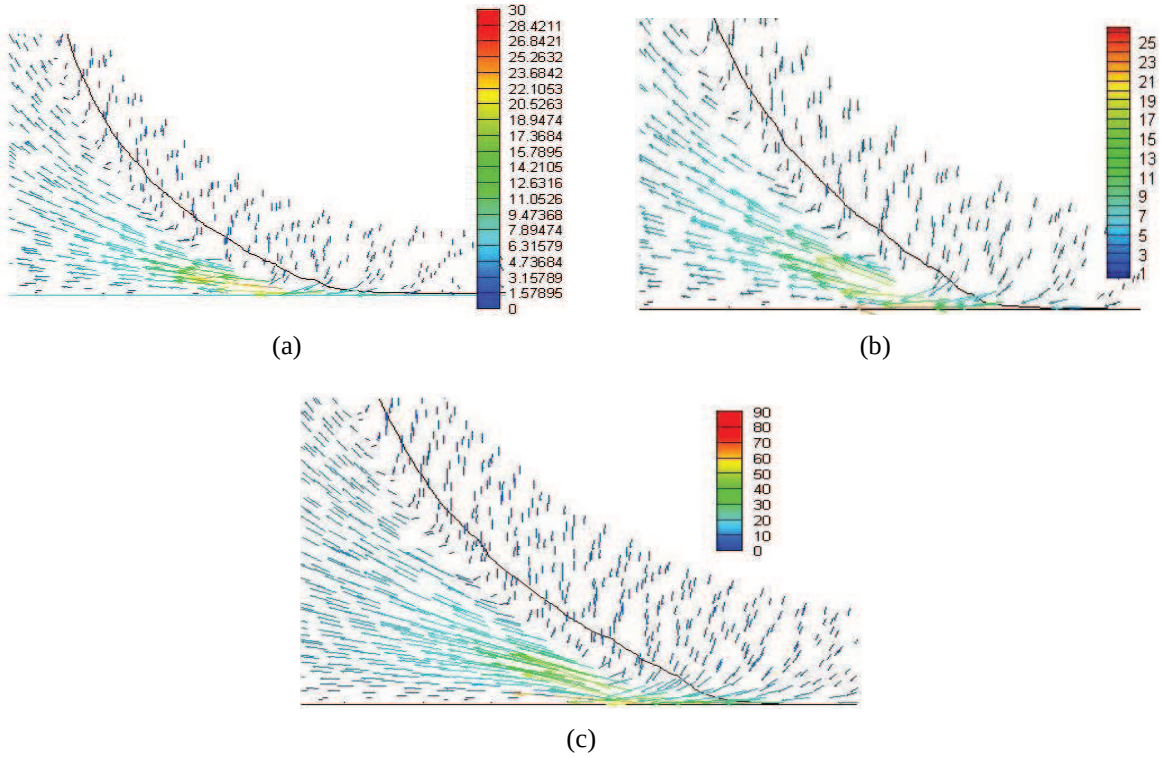

(a) (b)

(c)

FIG. 7: Velocity profiles of the air as the FC-72 droplets with 1.7 mm diameter initiate contact with flat surface: (a) V = 2 m/s at 1 atm pressure; (b) V = 2 m/s at 4 atm pressure; and (c) V = 5 m/s at 1 atm pressure.

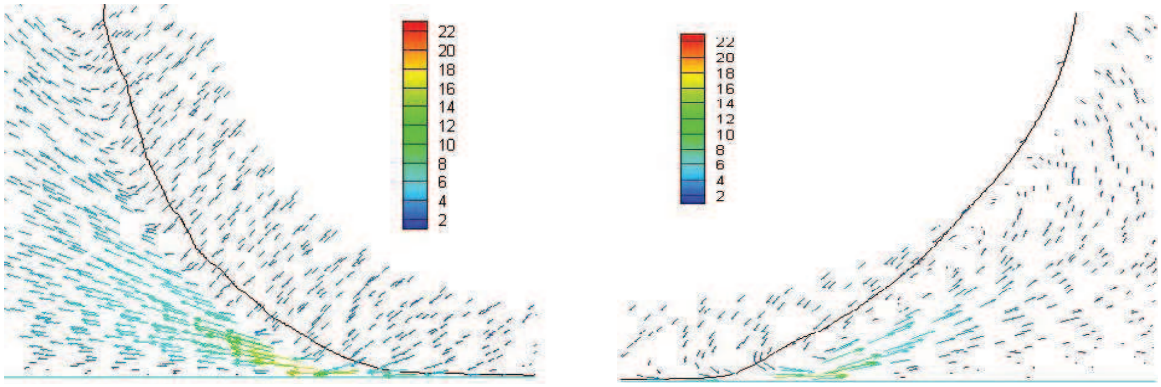

(a) (b)

FIG. 8: Velocity profile of FC-72 droplet with D = 1.7 mm and V = 2 m/s impact onto inclined surface with angle 45 deg: (a) downhill direction; (b) uphill direction.

with D = 1.7 mm impacting at V = 2 m/s on a horizontal surface. The maximum internal pressure at the moment of impact is 19 kPa. For V = 5 m/s, the maximum pressure increases to 160 kPa, as seen in Figure 9b. Note also that as the same droplet of D = 1.7 mm and V = 2 m/s impacts onto a 45 deg inclined surface, the maximum pressure reaches only 8.5 kPa, as seen in Fig. 9c.

5. ANALYSIS

5.1 Splashing Threshold

According to previous research, the pressure inside the droplet is generated during the process of impact or during the conversion of the momentum of the impacting

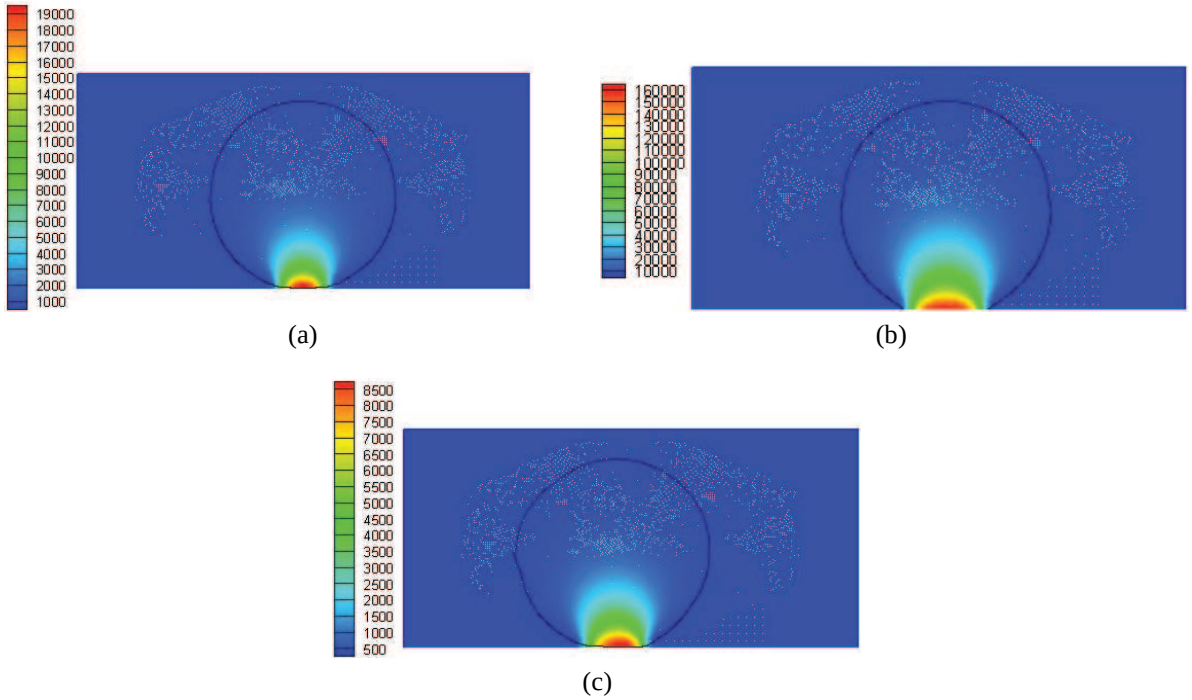

(a) (b)

(c)

FIG. 9: Pressure profile of droplet with 1.7 mm diameter initiating contact with impact surface: (a) V = 2 m/s at 1 atm; (b) V = 5 m/s at 1 atm; and (c) V = 2 m/s at 1 atm, 45 deg inclined surface.

droplet into the momentum of flow along the impact surface (Harlow and Shannon, 1967). Once the inside pressure exceeds the surface tension, splashing occurs. The most recognized theory that explains how pressure is generated in the droplet during droplet impact is the "water hammer" effect (Engel, 1955),

$$P = \rho V C_l \tag{1}$$

where ρ is the liquid density, V is the droplet impact velocity, and C_l is the speed of sound in the liquid. In the water hammer theory, the liquid on the contact area is compressed and pressure is generated as the shock wave propagates in the liquid with the speed of sound. Once the front of the shock wave reaches the free surface of the liquid droplet, spreading or splashing is initiated. Therefore, the pressure due to the impact initiates splashing. However, this analysis only considered the cases in which the droplet impact velocity was over 100 m/s. Xu et al. (2005) modified Eq. (1), and the pressure due to the water hammer effect for low-impact velocity was expressed as

$$P \sim \rho_g V_S C_g \tag{2}$$

Where ρ_g is the gas density, V_s is the spreading velocity after droplet impact on a solid surface, and C_g is the speed of sound in the gas. Considering the ideal gas formulation, ρ_g can be written as

$$\rho_g = \frac{pM_m}{R_u T} \tag{3}$$

where p is the ambient gas pressure, M_m is the molecular weight of the gas, R_u is the universal gas constant (8314 N m/kg mol K), and T is the gas temperature. The speed of sound in the gas is expressed as

$$C_g = \sqrt{\frac{nR_u T}{M_m}} \tag{4}$$

where n is the adiabatic constant for a compressible gas. The velocity of the spreading edge is

$$V_S = \sqrt{\frac{DV}{4t}} \tag{5}$$

Thus, the pressure caused by the shock wave can be expressed as

$$P \sim \rho_g C_g V_S = \frac{pM_m}{R_u T} \cdot \sqrt{\frac{nR_u T}{M_m}} \cdot \sqrt{\frac{DV}{4t}} \tag{6}$$

The stress caused by the surface tension can be expressed as

$$\tau_{\mathrm{ST}} = \frac{\sigma}{h} = \frac{\sigma}{\sqrt{\nu t}} \tag{7}$$

where σ is the surface tension, h is the thickness of the liquid layer, and ν is the kinematic viscosity of the liquid. Thus, the splash occurs when the ratio of

$$P/\tau_{\mathrm{ST}} \sim \sqrt{nM_m}p \cdot \sqrt{\frac{DV}{4R_u T}} \frac{\sqrt{\nu}}{\sigma} > S_{\mathrm{critical}} \tag{8}$$

From experimental results, S_{critical} was found to be 0.45 (Xu et al., 2005). Interestingly, Eqs. (5) and (6) show that P should increase proportionally with V_s, and the empirical correlation expressed by Eq. (8) shows that, provided the P/τ_{ST} ratio exceeds S_{critical}, splashing should occur. That is, Eq. (8) can predict the splashing threshold of droplets impacting against flat horizontal surfaces for any given ambient pressure p and impact velocity V. However, this prediction is in contradiction with our experimental results on inclined surfaces (Fig. 6), which show that as V_s increases with steeper angles, splashing is reduced.

Until now, the most accepted explanation has been that splashing occurs once the momentum of the droplet cannot be converted into the momentum of flow along the surface (Levin and Hobbs, 1970). Although the droplet impact is a dynamic and transient process, we simplified the impact analysis by assuming that the droplet impact was a pseudo–steady state process, as shown in Fig. 10, to illustrate the effects of droplet velocity and impact angle on the pressure variation inside the droplet. During this pseudo–steady state impact process, the momentum variation of the droplet at contact with the impact surface can be expressed as

$$\frac{dm\vec{V}_n}{dt} = \vec{F} = P\left(\pi r^2\right) \tag{9}$$

where $\vec{V}_n$ and P are the velocity and pressure of the droplet normal to the impact surface, respectively, and r

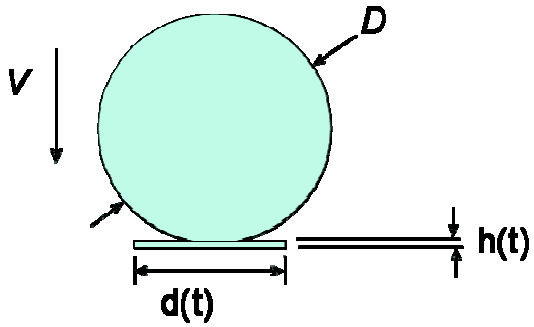

FIG. 10: Sketch of the spreading after droplet impact onto rigid flat surface.

is the radius of the spreading layer defined as (Vander Wal et al., 2006)

$$r(t) = R_m\left(1 - e^{-t/t_c}\right) \tag{10}$$

In Eq. (10), R_m is the maximum spreading radius, which can be expressed as (Pasandideh-Fard et al., 2002)

$$R_m = \frac{D}{2}\sqrt{\frac{\mathrm{We}+12}{3\left[1-\cos(\theta)\right]+4\left(\mathrm{We}/\sqrt{\mathrm{Re}}\right)}} \tag{11}$$

where t_c is the characteristic spreading time, which is given as the time from initial droplet contact to maximum spreading. The value can be defined as $8D/3V$ (Pasandideh-Fard et al., 1998). The mass of the spreading can be expressed as

$$\pi\left[r(t)\right]^2 h(t)\,\rho \tag{12}$$

Inserting Eqs. (10)–(12) into the left-hand side of Eq. (9) and simplifying,

$$P = \left|\vec{V}_n\right|\sqrt{\rho\mu}\left(\frac{2e^{-t/t_c}\sqrt{t}}{t_c\left(1-e^{-t/t_c}\right)}+\frac{1}{2\sqrt{t}}\right) \tag{13}$$

The numerical simulation shown in Fig. 9 demonstrates that the pressure inside the droplet increases with increasing $\vec{V}_n$. The ratio of the pressure caused by a sudden change of momentum to the shear stress caused by the surface tension shown in Eq. (7) can be expressed as

$$\frac{P}{\tau_{\mathrm{ST}}} = \frac{P}{\left(\sigma/\sqrt{\nu t}\right)} = \frac{\left|\vec{V}_n\right|\mu}{\sigma}\left[\frac{2e^{-t/t_c}t}{t_c\left(1-e^{-t/t_c}\right)}+\frac{1}{2}\right]$$
$$\approx 2.5\frac{\mathrm{We}_n}{\mathrm{Re}_n} = 2.5\mathrm{Ca}_n \tag{14}$$

Figure 3 shows that the ambient pressure also affects the threshold of the splashing. Therefore, to predict the threshold of splashing (S_{critical}), we propose the following power law correlation, which must yield a value larger than 0.45 according to previous studies (Xu et al., 2005):

$$S_{\mathrm{critical}} \sim c_1\left(\mathrm{Ca}_n\right)^{c_2}\left(\frac{p}{P_o}\right)^{c_3} > 0.45 \tag{15}$$

where p is the environmental gas pressure and P_o is the atmospheric pressure. Vander Wal et al. (2006) found a similar splashing threshold dependence on Ca_n, with its exponent equal to 0.5. Using this value for c_2 and applying the experimental results, we obtain

$$2.84\left(\mathrm{Ca}_n\right)^{0.5}\left(\frac{p}{P_o}\right)^{0.42} > 1 \tag{16}$$

Figure 11 shows the comparison of experimental results with the model predictions at atmospheric pressure. Because the threshold of splashing $2.84(\mathrm{Ca}_n)^{0.5}(p/P_o)^{0.42}$ equals 1, the splashing and no-splashing zones are clearly divided. Vander Wal et al. (2006) varied the droplet diameter and fluid properties to determine the splashing threshold. As shown in Fig. 11, Vander Wal's experimental data distribute evenly around the threshold of 1.

Figure 12 shows the comparison between model simulations and our experimental results of the splashing threshold as a function of normalized pressure. It shows that for subatmospheric pressures, Ca for the splashing threshold drops dramatically, but it decreases gradually as the pressure increases above atmospheric. For subatmospheric pressures, Xu's experimental data (2007) also show strong agreement with the correlation proposed by Eq. (16).

5.2 Kelvin-Helmholtz Instability

The mechanism of the splashing phenomenon is explained by K-H instability theory, which occurs when shear stress is present within a continuous fluid or when there is sufficient velocity difference across the interface

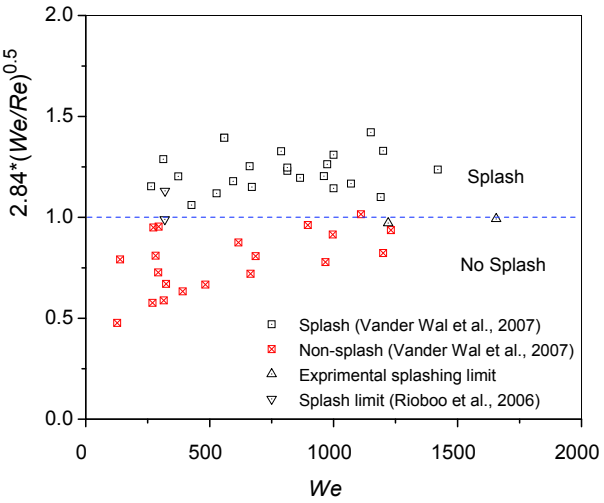

FIG. 11: Model-predicted splashing limit versus experimental results.

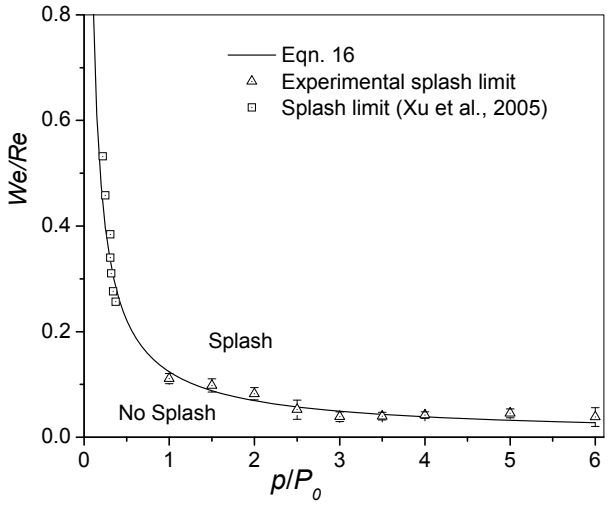

FIG. 12: Model-predicted splashing limit versus experimental results.

between two fluids (Jepsen et al., 2006; Yoon and Desjardin, 2006). The dispersion relationship of K-H instability can be expressed as

$$\omega^2 = \frac{\rho_g}{\rho} V_{\rm rel}^2 k^2 - \frac{\sigma}{\rho} k^3 \tag{17}$$

where ω is the interface growth rate, k is the wave number, σ is the surface tension of the liquid; ρ and ρ_g represent the densities of the liquid and gas, respectively, and $V_{\rm rel}$ is the relative velocity between the spreading droplet and surrounding gas. The k corresponding to the maximum growth rate $\omega_{\max}$ can be obtained when the derivative of k on the right-hand side of Eq. (17) is set to zero, and expressed as

$$k_{\max} = \frac{2V_{\rm rel}^2 \rho_g}{3\sigma} \tag{18}$$

Equations (17) and (18) show that as $V_{\rm rel}$ increases, both $k_{\max}$ and $\omega_{\max}$ increase (Jepsen et al., 2006). An analogous increase results as the ambient gas density ρ_g increases. Considering the ambient air as an ideal gas, the relationship between the gas pressure and density can be expressed as

$$p = \rho_g R_u T \tag{19}$$

Thus, Eq. (18) also illustrates that as the ambient pressure increases, the strength of the instabilities increase as well. This is congruent with experimental evidence, shown in Figs. 3 and 4, that the splashing angle increases with the increase of the ambient pressure. The K-H instability is determined by the molecular force between the two fluids moving at a relative velocity. Macroscopically, this molecular force is expressed as the shear stress. As the density of the air increases, the number of air molecules in the surrounding volume increases. Inevitably, the stress increases as well. As a result, the splashing or instability increases with the increase of the ambient gas pressure, as observed in our experiments.

An apparent paradox appears in Figs. 5 and 6, which show that as the inclined angle increases, the splashing weakens, although the spreading velocities V_s increase in the downhill direction. According to Eq. (18), instabilities or splashing at 45 deg should be stronger than that at 15 deg under the assumption that the velocity of the ambient gas during droplet impact is 0 and $V_{\rm rel}$ is equal to V_s (Sikalo et al., 2005; Rioboo et al., 2006).

This apparent paradox may be reconciled by examining Figs. 7 and 8. Clearly, the velocity of the ambient air near the droplet impact area is much greater than the spreading velocity. Also, the ambient air moves at a certain angle with respect to the impact surface and thus can have velocity normal to the impact surface. Furthermore, for the same impact velocity, the angle of the ambient air velocity vector increases as the ambient pressure increases (Figs. 7a and 7b). Therefore, with the understanding of ambient air movement, $V_{\rm rel}$ not only provides a reasonable solution to the above paradox, but it also explains why the splashing droplets move at an inclined angle relative to the impact surface, which varies with ambient pressure (Fig. 4).

The K-H instability analysis [Eq. (18)] not only provides a better explanation of the mechanism of splashing, but it also shows good agreement with the splashing threshold correlation analysis shown by Eq. (16). First, both analyses show that as the surface tension decreases, the possibility of splashing increases. Namely, with decreasing σ, $k_{\max}$ increases [see Eq. (18)] as well as the value of $2.84(\mathrm{Ca}_n)^{0.5}(p/P_o)^{0.42}$. Conversely, with increasing ρ_g, $k_{\max}$ increases [see Eq. (18)] and so does the value of $2.84(\mathrm{Ca}_n)^{0.5}(p/P_o)^{0.42}$. Finally, although the quantitative relationship between $V_{\rm rel}$ and $\vec{V}_n$ cannot be directly determined from Eqs. (16) and (18), the results of our numerical simulations (Figs. 7 and 8) show that as $\vec{V}_n$ increases, $V_{\rm rel}$ increases as well.

6. CONCLUSIONS

1. The threshold of splashing on a smooth, flat surface has been examined under a wide We range under

varying air pressures and oblique impact angles. Increasing We increases the magnitude of splashing, confirming the results of previous studies. The effect of air pressure on splashing, first studied by Xu et al. (2005) and Xu (2007), has been verified to extend into superatmospheric conditions. Increasingly oblique impact angles appeared to reduce splashing.

2. A new semiempirical splash threshold correlation was derived, considering the internal pressure generation during droplet impact and the opposing, retentive surface tension. The correlation is similar in form to Vander Wal's (2006), but extends the range of applicability to nonatmospheric air pressures. The decrease in splashing observed in oblique impacts is accounted for by using $\vec{V}_n$.

3. According to Xu's results, splashing should increase with increasing spreading velocity V_s. However, our experimental evidence demonstrated that with increasingly oblique impact angles, spreading velocity increases, but splashing reduces. This apparent paradox is resolved by our re-examination of K-H instability theory and numerical analyses, which shows that the occurrence of splashing is more attributable to V_{rel}, the relative velocity between the spreading droplet and the surrounding gas. Thus, the air motion initiated by the impacting droplet cannot be neglected. V_{rel} appears to scale well with $\vec{V}_n$ used in our correlation, although a direct quantitative relation was not obtained.

REFERENCES

Allen, R. F., Role of surface-tension in splashing, *J. Colloid Interface Sci.*, vol. 51, no. 2, pp. 350–351, 1975.

Allen, R. F., The mechanics of splashing, *J. Colloid Interface Sci.*, vol. 124, no. 1, pp. 309–316, 1988.

Bowden, F. P. and Field, J. E. Brittle fracture of solids by liquid impact by solid impact + by shock, *Proc. R. Soc. London Ser. A*, vol. 282, no. 139, pp. 331–352, 1964.

Engel, O. G., Waterdrop collisions with solid surfaces, *J. Res. Nat. Bur. Stand.*, vol. 54, no. 5, pp. 281–298, 1955.

Field, J. E., ELSI Conference: Invited lecture—Liquid impact: Theory, experiment, applications, *Wear*, vol. 235, pp. 1–12, 1999.

Field, J. E., Lesser, M. B., and Dear, J. P., Studies of two-dimensional liquid-wedge impact and their relevance to liquid-drop impact problems, *Proc. R. Soc. Lond Ser. A*, vol. 401, no. 1821, pp. 225–249, 1985

Fujimoto, H., Shiotani, Y., Tong, A. Y., Hama, T., and Takuda, H., Three-dimensional numerical analysis of the deformation behavior of droplets impinging onto a solid substrate, *Int. J. Multiphase Flow*, vol. 33, no. 3, pp. 317–332, 2007.

Harlow, F. H. and Shannon, J. P., Splash of a liquid drop, *J. Appl. Phys.*, vol. 38, no. 10, pp. 3855–3866, 1967.

Hobbs, P. V. and Kezweeny, A. J., Splashing of a water drop, *Science*, vol. 155, no. 3766, pp. 1112–1114, 1967.

Hobbs, P. V. and Osheroff, T., Splashing of drops on shallow liquids, *Science*, vol. 158, no. 3805, pp. 1184–1186, 1967.

Jepsen, R. A., Yoon, S. S., and Demosthenous, B., Effects of air on splashing during a large droplet impact: experimental and numerical investigations, *Atomization and Sprays*, vol. 16, no. 8, pp. 981–996, 2006.

Josserand, C., Lemoyne, L., Troeger, R., and Zaleski, S., Droplet impact on a dry surface: Triggering the splash with a small obstacle, *J. Fluid Mech.*, vol. 524, pp. 47–56, 2005.

Kang, B. S. and Lee, D. H., On the dynamic behavior of a liquid droplet impacting upon an inclined heated surface, *Exp. Fluids*, vol. 29, no. 4, pp. 380–387, 2000.

Kim, H. Y., Feng, Z. C., and Chun, J. H., Instability of a liquid jet emerging from a droplet upon collision with a solid surface, *Phys. Fluids*, vol. 12, no. 3, pp. 531–541, 2000.

Lesser, M. B., Analytic solutions of liquid-drop impact problems, *Proc. R. S. London A*, vol. 377, no. 1770, pp. 289–308, 1981.

Lesser, M. B. and Field, J. E., The impact of compressible liquids, *Annu. Rev. Fluid Mech.*, vol. 15, pp. 97–122, 1983.

Levin, Z. and Hobbs, P. V., Charge separation due to splashing of water drops, *B. Am. Meteorol. Soc.*, vol. 51, no. 6, pp. 577–586, 1970.

Levin, Z. and Hobbs, P. V., Splashing of water drops on solid and wetted surfaces—Hydrodynamics and charge separation, *Philos. Trans. R. Soc. S-A*, vol. 269, no. 1200, pp. 555–585, 1971.

Li, X. Y., Ma, X. H., and Lan, Z., Behavioral patterns of drop impingement onto rigid substrates with a wide range of wettability and different surface temperatures, *AICHE J.*, vol. 55, no. 8, pp. 1983–1992, 2009.

Mundo, C., Sommerfeld, M., and Tropea, C., Droplet-wall collisions—Experimental studies of the deformation and breakup process, *Int. J. Multiphase Flow*, vol. 21, no. 2, pp. 151–173, 1995.

Pasandideh-Fard, M., Bhola, R., Chandra, S., and Mostaghimi, J., Deposition of till droplets on a steel plate: Simulations and experiments, *Int. J. Heat Mass. Trans.*, vol. 41, no. 19, pp. 2929–2945, 1998.

Pasandideh-Fard, M., Pershin, V., Chandra, S., and Mostaghimi, J., Splat shapes in a thermal spray coat-

ing process: Simulations and experiments, *J. Therm. Spray Technol.*, vol. 11, no. 2, pp. 206–217, 2002.

Prunet-Foch, B., Legay, F., Vignes-Adler, M., and Delmotte, C., Impacting emulsion drop on a steel plate: Influence of the solid substrate, *J. Colloid Interface Sci.*, vol. 199, no. 2, pp. 151–168, 1998.

Range, K. and Feuillebois, F., Influence of surface roughness on liquid drop impact, *J. Colloid Interface Sci.*, vol. 203, no. 1, pp. 16–30, 1998a.

Range, K. and Feuillebois, F., Splashing of a drop on a rough surface, *High Temp. Mater. Process.*, vol. 2, no. 2, pp. 287–300, 1998b.

Rein, M., The transitional regime between coalescing and splashing drops, *J. Fluid Mech.*, vol. 306, pp. 145–165, 1996.

Rioboo, R., Adao, M. H., Voue, M., and De Coninck, J., Experimental evidence of liquid drop break-up in complete wetting experiments, *J. Mater. Sci.*, vol. 41, no. 16, pp. 5068–5080, 2006.

Rioboo, R., Bauthier, C., Conti, J., Voue, M., and De Coninck, J., Experimental investigation of splash and crown formation during single drop impact on wetted surfaces, *Exp. Fluids*, vol. 35, no. 6, pp. 648–652, 2003.

Rioboo, R., Tropea, C., and Marengo, M., Outcomes from a drop impact on solid surfaces, *Atomization and Sprays*, vol. 11, no. 2, pp. 155–165, 2001.

Sikalo, S., Tropea, C., and Ganic, E. N., Dynamic wetting angle of a spreading droplet, *Exp. Therm. Fluid Sci.*, vol. 29, no. 7, pp. 795–802, 2005.

Stow, C. D. and Hadfield, M. G., An experimental investigation of fluid-flow resulting from the impact of a water drop with an unyielding dry surface, *Proc. R. Soc. London A*, vol. 373, no. 1755, pp. 419–441, 1981.

Vander Wal, R. L., Berger, G. M., and Mozes, S. D., The splash/non-splash boundary upon a dry surface and thin fluid film, *Exp. Fluids*, vol. 40, no. 1, pp. 53–59, 2006.

Worthington, A., On the forms assumed by drops of liquids falling vertically on a horizontal plate, *Proc. R. Soc. London*, vol. 25, pp. 261–271, 1876.

Xu, L., Liquid drop splashing on smooth, rough, and textured surfaces, *Phys. Rev. E*, vol. 75, no. 5, pp. 26–28, 2007.

Xu, L., Zhang, W. W., and Nagel, S. R., Drop splashing on a dry smooth surface, *Phys. Rev. Lett.*, vol. 94, no. 18, pp. 505–516, 2005.

Yoon, S. S. and DesJardin, P. E., Modelling spray impingement using linear stability theories for droplet shattering, *Int. J. Numer. Methods Fluids*, vol. 50, no. 4, pp. 469–489, 2006.

Yoon, S. S., Jepsen, R., James, S. C., Liu, J., and Aguilar, G., Are drop-impact phenomena described by Rayleigh-Taylor or Kelvin-Helmholtz theory?, *Drying Technol.*, vol. 27, pp. 1–6, 2009.

Yoon, S. S., Jepsen, R. A., Nissen, M. R., and O'Hern, T. J., Experimental investigation on splashing and nonlinear finger-like instability of large water drops, *J. Fluid Struct.*, vol. 23, no. 1, pp. 101–115, 2007.